

PATTERNS OF SUSPENDED MATTER IN THE EAST FRISIAN WADDEN SEA: COMPARISON OF NUMERICAL SIMULATIONS WITH MERIS OBSERVATIONS

Nina Gemein¹, Emil Stanev², Gerold Brink-Spalink², Jörg-Olaf Wolff² and Rainer Reuter¹

1. Carl von Ossietzky University of Oldenburg, Institute of Physics, 26111 Oldenburg, Germany; [nina.gemein / rainer.reuter}@uni-oldenburg.de](mailto:{nina.gemein / rainer.reuter}@uni-oldenburg.de)
2. Carl von Ossietzky University of Oldenburg, Institute for Chemistry and Biology of the Marine Environment (ICBM), 26111 Oldenburg, Germany; [e.stanev / wolff}@icbm.de](mailto:{e.stanev / wolff}@icbm.de)

ABSTRACT

The transport of suspended matter in the East Frisian Wadden Sea is investigated using satellite observations and numerical simulations. Satellite data originate from the Medium Resolution Imaging Spectrometer (MERIS) onboard the ESA satellite ENVISAT and have a spatial resolution of 300 m. The numerical model is based on the General Estuarine Transport Model (GETM); it has a horizontal resolution of 200 m and ten depth layers and is coupled with a suspended matter transport model. Numerically simulated and observed data sets have a comparable resolution. As it is much higher than any known resolution of earlier investigations covering the entire area of the East Frisian Wadden Sea, new patterns of suspended matter distribution could be discovered. They are consistent in the two data sets and reveal an oscillatory behaviour of sediment pools northward of the backbarrier basins and clear propagation patterns of tidal water outflow into the North Sea. The agreement between observations and simulations gives a convincing proof that the model simulates the basic dynamic processes, which motivates its further use for operational purposes in the coastal zone.

Keywords: ocean colour, suspended matter, current modelling, sediment transport modelling.

INTRODUCTION

The transport of suspended matter in seawater is an important part of coastal physical oceanography. The recent progress in this research area is largely due to the new *in situ* instrumentation, e.g. the Acoustic Doppler Current Profiler (ADCP) (1), transmissometry and radiometry (2) and ocean colour sensors onboard satellites (3,4), which made it possible to observe temporal variability of suspended sediment concentrations at different depths in the water column and over large areas. Supported by results of numerical modelling, these new generation observations can reveal detailed information on the near coastal hydro- and suspended matter dynamics. In this paper we demonstrate the usefulness of combining remote sensing and numerical modelling when studying the oceanographic processes in the Wadden Sea.

Traditionally, data from the Wadden Sea originate from ship surveys, as well as from tide gauges and other time series stations. The former data do not resolve the complex dynamics spatially, the latter give information about the temporal variability of the water level only, in some cases temperature and salinity data at several depths are also provided (5,6). Information on spatial patterns is provided by numerical models. However, a detailed validation of numerical models against observations is needed not only at fixed locations but also over larger areas. It appears that satellite images with the capability of resolving small-scale structures far below 1 km can be efficiently used for this purpose since they resolve the basic hydrodynamic features in the tidal flat areas.

A fundamental characteristic of the Wadden Sea (Figure 1) is the vigorous suspended matter dynamics. The Medium Resolution Imaging Spectrometer (MERIS) onboard the ESA satellite ENVISAT with a 300 m ground resolution is able to detect total suspended matter (TSM) concentrations as well as yellow substance (YS) and chlorophyll (CHL) in the upper water layer. Since the TSM signals measured with MERIS contain information on both, advection and turbulence, they provide an important source of data for model validation. The spatial patterns associated with sus-

pendent sediment transport have recently been numerically simulated with a realistic (3-D) circulation model, the General Estuarine Transport Model (GETM) coupled with a sediment transport model (7). Our interest here is to use these simulations and to compare them with remote sensing imagery of the East Frisian Wadden Sea, which is the first step on the route to a validation of our model.

Ocean colour imagery in turbid coastal waters

An important application of remote sensing is the observation of ocean colour in coastal zones, which facilitates the understanding of important hydrodynamic and suspended matter processes.

The large variations of the suspended matter concentration in tidal flat regions such as the Wadden Sea imply the need for multispectral measurements for the separation of the different water constituents. This is important especially in the near infrared (NIR). Bands in the NIR are used for the correction of atmospheric contributions to the visual bands (VIS), which is essential for a proper detection of water constituents. The principal procedure, known as dark pixel method, is to measure the radiance in the near infrared and to assume that there is no contribution coming out of the water column because of the strong absorption of water at these wavelengths (8). Therefore, the signal should originate from scattering in the atmosphere only. However, this assumption is wrong over turbid coastal waters (case-2 waters). Suspended matter is able to backscatter the radiation near the surface before it is absorbed in the near-surface water layer. As a consequence, the atmospheric correction can lead to negative values of calculated reflectances in the visible bands. There is thus a high demand for improvements of data processing regarding the atmospheric correction in coastal zones (9). Compared with all former satellites, MERIS, with its many spectral bands, especially in the NIR region, provides the best possibilities for good atmospheric correction. Therefore it gives a much better accuracy for water constituent determination compared with sensors of higher spatial resolution, e.g. SPOT and LANDSAT (10,11), which are not specialised for water constituents.

For open ocean images (case-1 waters) a ground resolution of one kilometre may be sufficient. However, the geometry of the islands cannot be well represented with this resolution. Furthermore, the dominating patterns of the water constituents also reveal scales much finer than one kilometre in the tidal basins.

Currently well established ocean colour sensors such as MODIS and SeaWiFS, having spatial resolution of 1000 m and 1100 m respectively, do not satisfy this requirement. Beside this, the swath width should be not less than 100 km for a good coverage of the whole area. Furthermore, for direct applications automatic data processing and algorithms for reliable level-2 data in coastal zones should be available. It is also of utmost importance that data should be delivered in near real-time to enable follow-up activities such as event-controlled water sampling or optimisation of ship cruise tracks during oceanic surveys by using the most actual satellite data.

At present, MERIS is only one sensor in space which is able to cope in principle with these needs. All other sensors fail at least in one of the requirements. Most of the current ocean colour sensors in space do not have a satisfying spatial resolution for this purpose. Other sensors fail in other points. MMRS, for example, has a ground resolution of 175 m, but with only 5 broad bands (20 to 150 nm in width) it does not have the spectral qualities needed (12). Furthermore, a nine-day repeat cycle is far too long for our purpose, because the region is often covered by clouds. So, the chance to get an adequate number of analysable images is very low. The only sensor that comes close to MERIS in its properties is OCM, having a spatial resolution of 350 m, global coverage in two days, with eight bands and 20 nm bandwidth for the first six bands (13).

MERIS is a hyperspectral sensor with a ground resolution of approx. 300 m for full resolution images. The images are taken by the so-called push-broom method. Five cameras cover the across-track direction with a 68.5° field of view, corresponding to 1,150 km at nadir, and scan the earth's surface while the satellite moves along-track. The spectrometers create a bi-dimensional image on the CCD arrays. One dimension is the spatial extension, the other is the spectrum, from 390 to 1040 nm in 15 programmable bands (14). The data run through several processing steps in the onboard analogue and digital electronics systems before the signal is sent to a ground station,

where the processing continues. The revisiting time of ENVISAT is two days for latitudes $>50^\circ$ (9). Scenes of the research area, located around $53^\circ43'N$ and $007^\circ30'E$, are taken regularly by ESA. So on the average, one scene is available every second day. The data processing is based on an artificial neural network, which uses eight visible bands. Improvements on the data processing are planned to be made during the whole sensor lifetime. The only disadvantage is that the full-resolution data are not available in near real-time yet, although work is ongoing to improve this.

With this sensor, it is possible for the first time to trace small-scale features in the near coastal dynamics and to validate simulations with numerical models having a similar spatial resolution.

Coastal waters suspended sediment transport models

With respect to physical oceanography, aspects of sediment dynamics are still in their infancy, although much experience already exists in the field of theory of processes close to the seabed, coastal engineering, stratigraphy, etc. Among the major problems is the lack of experience in downscaling from regional to shelf (resolving the shelf boundary layer), parameterisation of unresolved processes, missing high quality data needed for validation of models over large areas.

Sediment transport capabilities need coastal forecasting models with improved forecast of ocean turbulence, which control transport of matter (biological matter and sediment). The potential for improving models is strongly related to the availability of new measurement techniques for resolving sediment dynamics (e. g. backscatter signals from ADCP and fine resolution satellite data, the latter being the major subject of this paper).

In the models, resolving ocean regions next to the coast means resolving the coastal boundary layer, which requires complex physics and very fine resolution. When approaching the coast, the importance of sediment dynamics increases because it becomes coupled with water-and-morphodynamics. However, sediment transport modelling capabilities are still limited with the exception of some site-specific studies. We believe that the area of our investigation is such an exception. In a recent study (7), where a sediment transport model has been presented for the same region, the major interest was on the interaction between transport and turbulence. It is demonstrated that the turbulent kinetic energy is one of the main drivers of the dynamics of suspended particulate matter. Its absolute maxima are observed in the tidal inlets and their funnel-like extensions. The minima are in the backbarrier area coinciding approximately with the watersheds separating the individual basins. During most of the time, the entire water column shows a high level of turbulence. Only during slack water (duration of ~ 1 hour) the velocity reduces drastically and the level of turbulence diminishes, which enables the deposition of sediment.

Although the temporal variability of turbulence is of utmost importance for the sediment dynamics, it is not enough for correct predictions. As it has been demonstrated in (7), the combined impact of transport and turbulence is very important, proving that local models, which do not sufficiently resolve advection, would hardly resolve the dominating temporal patterns. The relative role of turbulent kinetic energy increases in the tidal channels where the response of sediment concentration to tidal forcing shows two maxima associated with flood and ebb currents. North of the barrier-islands, where the impact of transport is dominant, the variability pattern is uni-modal. Furthermore, it has been demonstrated in (7) that the three-dimensional structure of transport and turbulence has a very strong impact on the sediment dynamics, which proves that two-dimensional models having been widely used in the past research could hardly resolve all important characteristics of sediment dynamics. What has not been done in the previous studies is the validation of the numerical model over the entire East Frisian Wadden Sea. This is one of the main subjects addressed in the present paper.

METHODS

Observational area

The East Frisian Wadden Sea is characterised by a series of barrier-islands, each being a few kilometres long in east-west direction and one or two kilometres broad (Figure 1). This is a highly dynamic tidal area, where the conditions in the water column vary widely with season, tide, and

meteorological conditions. A fundamental characteristic of the Wadden Sea is the vigorous suspended matter dynamics. For example, up to 7200 tons of mud and 4300 tons of sand are moved in and out of the tidal channel of Otzumer Balje (Figure 1) over one tidal cycle (1). Therefore the water, especially in the backbarrier tidal flats, is characterised by high loads of suspended matter, which often reach concentrations of about 100 mg/l. Typical Secchi depths in this flat area are 0.1 to 0.5 m, depending on water depth, tide current, ground material, and wind force. They increase with increasing water depths. In the inlets they may reach a few metres at very clear water conditions.

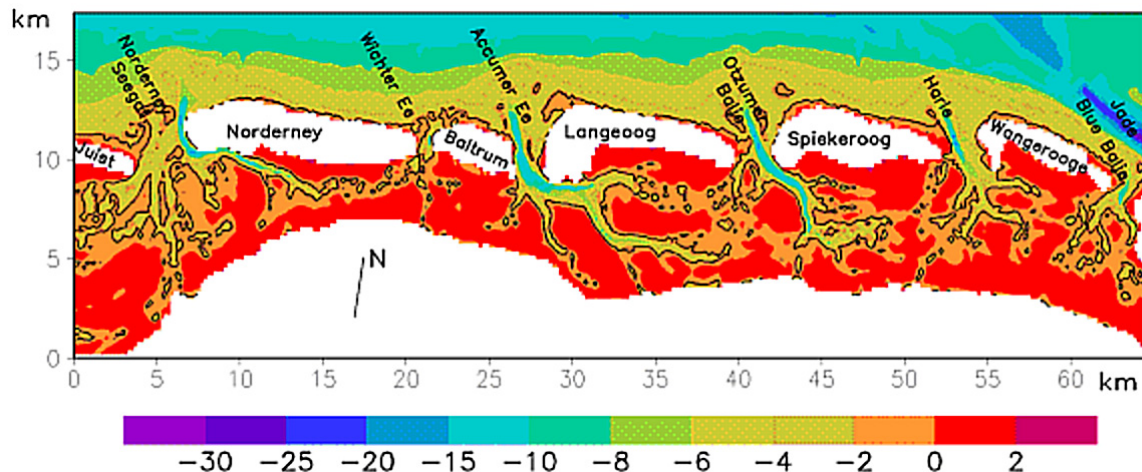


Figure 1: Topography of the East Frisian Wadden Sea used in the numerical model. The coordinates of the lower left corner are approximately $53^{\circ}36'N$ and $007^{\circ}05'E$. The isobaths are represented as negative numbers in units of metres below the mean sea-level. The arrow giving the direction to the North demonstrates that the model area is rotated, which is done in order to reduce the size of the model grid. The -1.5 m isobath is also plotted, revealing approximately the dry area under low water.

MERIS data

MERIS scenes have been provided by ESA as level-2 products in full resolution. The delivered data are geo-referenced and contain an atmospheric correction. There are over 90 usable scenes for the research area by now, covering a time scale from June 2002 to April 2005. For the analysis of data and their graphical presentation the freely available BEAM-VISAT (Version 3.4.1) software (15) was used.

The operational data processor (IPF V4.06/4.07/4.10, (16,17) is based on a neural network (18), which has three angles and eight reflectances as input. The output consists of the concentrations of chlorophyll *a* (CHL) and total suspended matter (TSM), and of the absorption coefficient of yellow substance (YS) at 412 nm. Each pixel of the image has a quality indicator (flag) that informs the user if the pixel is considered valid or not.

The calibration of MERIS is found to be very accurate, thanks to the onboard radiometric calibration (19). The quality improvements of the product algorithms have led to several new processors with a newly trained neural network (20,21), but they are not operational yet. The processors produce good results especially in coastal areas. Compared with all sensors in the past, several bands in the IR allow highest accuracy of atmospheric correction (9). Unfortunately, all full-resolution (FR) data used in this paper are processed with the older processor version (up to IPF V4.10). In the meantime the new processor 5.02 is operational. Its results are not considered to be very satisfying (in terms of accurate concentrations) (e.g. 22,23). The radiometric accuracies for the surface reflectance given in the MERIS Product Handbook over ocean are $2 \cdot 10^{-4}$, for chlorophyll and total suspended matter 15% each, and 30% for yellow substance (24).

The flags for the validity of the water constituent concentrations are raised in the majority of cases in the Wadden Sea. Nevertheless, the observed patterns are considered to reflect the real surface distribution, which is sufficient for a validation of the model in the first step.

For the validation of MERIS derived suspended matter concentrations in the Wadden Sea, filtration data of ship cruises from 2003 to 2005 have been used. Only few data match in time, and these are data with low concentrations (Table 1). Only one point corresponds to a valid satellite pixel ($TSM_{MERIS} = 7.1\text{mg/l}$), but all points are considered to be reliable due to valid neighbouring pixels with consistent concentrations. The positions of the water sampling are always located inside the corresponding satellite pixel. One data point has a time delay of two tidal cycles between satellite data and sample filtration ($TSM_{MERIS} = 9.8\text{mg/l}$), therefore it should be treated with caution.

Table 1: MERIS derived TSM concentrations and TSM filtration data. Positions see Figure 1: OB = Otzumer Balje near Spiekeroog, SS = south of Spiekeroog, NWW = north-west of Wangerooge; A = temporally weighted values, calculated out of a series of samples, B = 1 day difference, but same tide phase.

Date	Position	TSM_{MERIS} / mg/l	$TSM_{Filtration}$ / mg/l	Remarks
23. Apr 03	OB	7.1	7.1	
11. Aug 03	OB	9.13	6.9	A
13. Aug 03	SS	19.56	17.9	A
9/10 Aug 2003	NWW	9.8	8.37	B
26. Apr 05	OB	9.82	13.2	A

The water samples were cooled and filtered on the same day or on the next day. Annealed glass fibre filters with $0.7\ \mu\text{m}$ porewidth were used for the filtration. At the end of the filtration they were rinsed with purified water to wash out the salt remaining in the filter, and then dried for two to three days at 60°C before the second weighing.

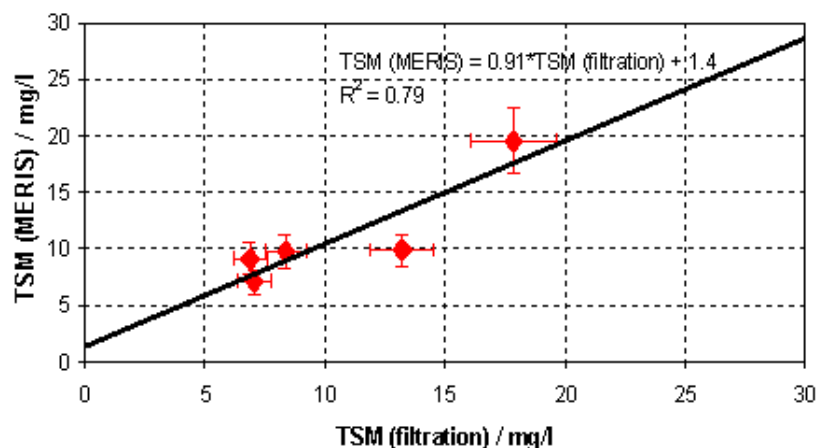


Figure 2: MERIS derived TSM concentrations versus TSM filtration data, taken at different times and locations in the Wadden Sea, see Table 1.

A direct comparison between these *in situ* point measurements and the $300\ \text{m} \times 300\ \text{m}$ MERIS pixels is naturally difficult, especially when having big concentration gradients near the coast. Secondly, the suspended sediment is cumulated in clouds ranging from centimetres to metres in size. This results in an error when *in situ* data are compared with the satellite data, the latter being averaged over an area much larger than the above-mentioned range. The fact that the two data types give similar results (at least at low concentrations) is therefore surprising.

Although the neural network has been trained for TSM concentrations of up to $72\ \text{mg/l}$, the error for concentrations of more than approx. $30\ \text{mg/l}$ is much larger than for lower concentrations. For the comparison of satellite and model data only TSM values of less than $30\ \text{mg/l}$ have been used.

TSM patterns derived from MERIS data

In summer, surface concentrations of *TSM* computed from satellite data (Figures 3-6) reveal three different regimes that dominate the suspended matter patterns: (a) tidal flats, (b) tidal inlets and the area northward of them, and (c) the open German Bight.

Regime “a” is characterised by extremely large concentrations of *TSM*. It is assumed that these large concentrations are related to very shallow depths. It is noteworthy that this area is also well pronounced on the north coasts of the backbarrier islands (Figure 6a).

The second regime (b) is dominated by transport and is traced by large suspended matter concentrations in the tidal inlets and the area just in front of them. These high concentrations are due to sediment “clouds” originating from the tidal basins and propagating northwards. It is noteworthy that under regime “b” relatively low concentrations are observed in the deepest parts of the inlets (Figures 4a, 6a). This result supports the theoretical concept that although the velocity is very high (~1 m/s), the concentration remains small because of large depths. This is a common feature of many estuaries and is due to the weaker tidal mixing in the core of the estuary.

TSM concentrations depend on the tidal phase, with maximum values during the time of highest current velocities. The shape of the area where regime “b” is dominating (extending towards the North Sea in front of tidal channels) reveals the major mechanisms dominating the sediment dynamics: back-and-forth propagation of suspended matter between tidal flats and North Sea, and lateral transport of sediment “clouds” ensuring high concentrations on the shallows up to the 20 m isobath (Figure 1).

Regime “c” may be called open North Sea regime. During summer, *TSM* concentrations are very low beyond the 20 m isobath (the concentration in the German Bight is ~1 mg/l or less).

The *TSM* patterns change not only with tide but also with the time of the year, and depend on wind and biological activity. Figures 3 and 4 are examples of typical summer situations. The *TSM* concentrations show a strong gradient in front of the islands. The water originating from the inlets does not transport the suspended matter very far. Due to the biological processes in summer, the particles are glued together to aggregates and sink faster than normally (25,26). They vanish from the surface as soon as the current slows down after passing the inlet.

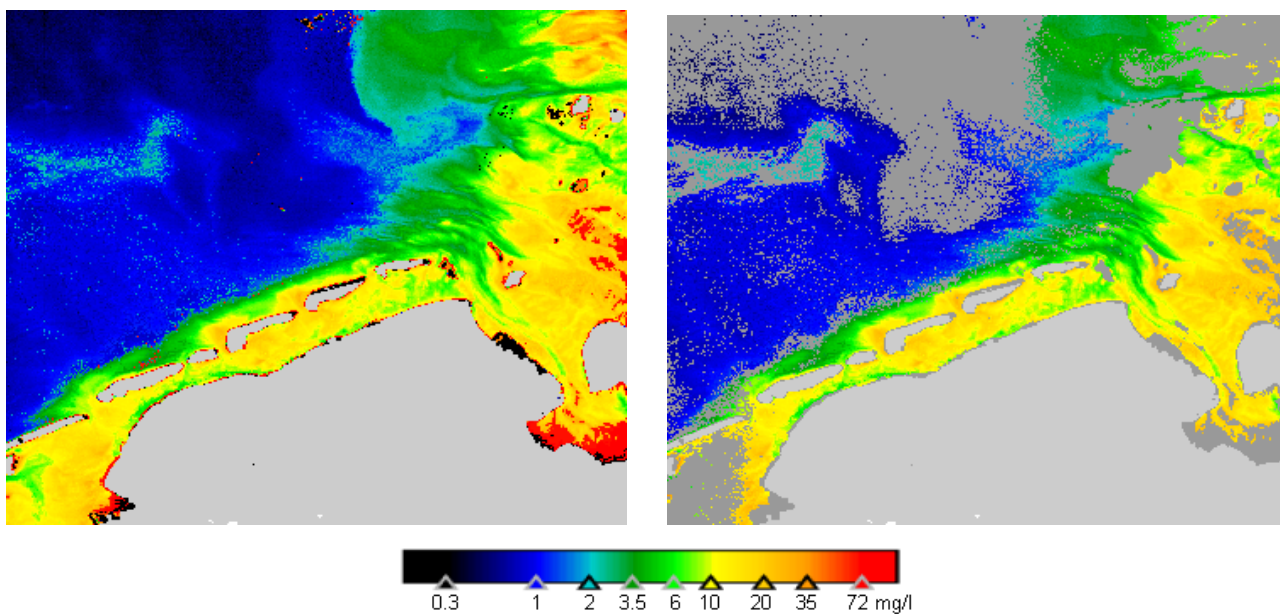


Figure 3: MERIS derived full-resolution *TSM* concentration image for 03 Jun 2004, taken during high water. An east/north-east wind was blowing over the area at 3.5 m/s for at least 12 hours before the image was taken. As in the following images, grey pixels are the land mask, white pixels are clouds. The left image shows all pixels as valid data, while in the right one all pixels considered by the algorithm to be invalid are dark grey.

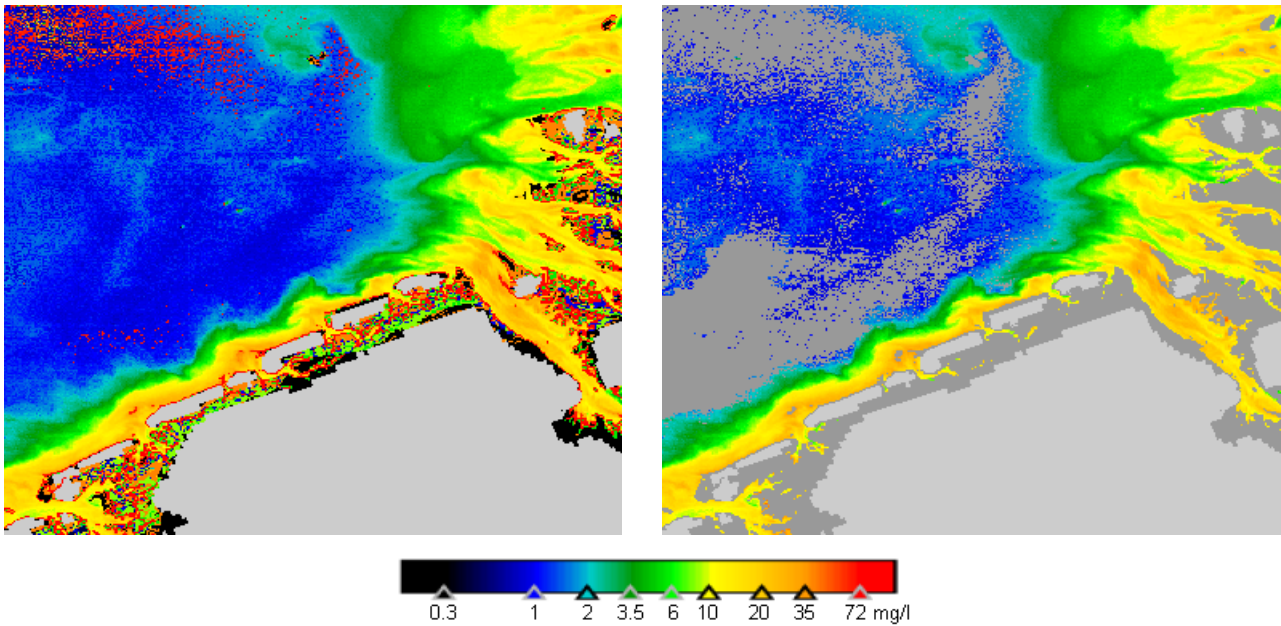


Figure 4: MERIS derived full-resolution TSM concentration image for 09 Sep 2004, taken 1.5 hours before low water. An east wind was blowing over the area at 5.5 m/s for at least 12 hours before the image was taken.

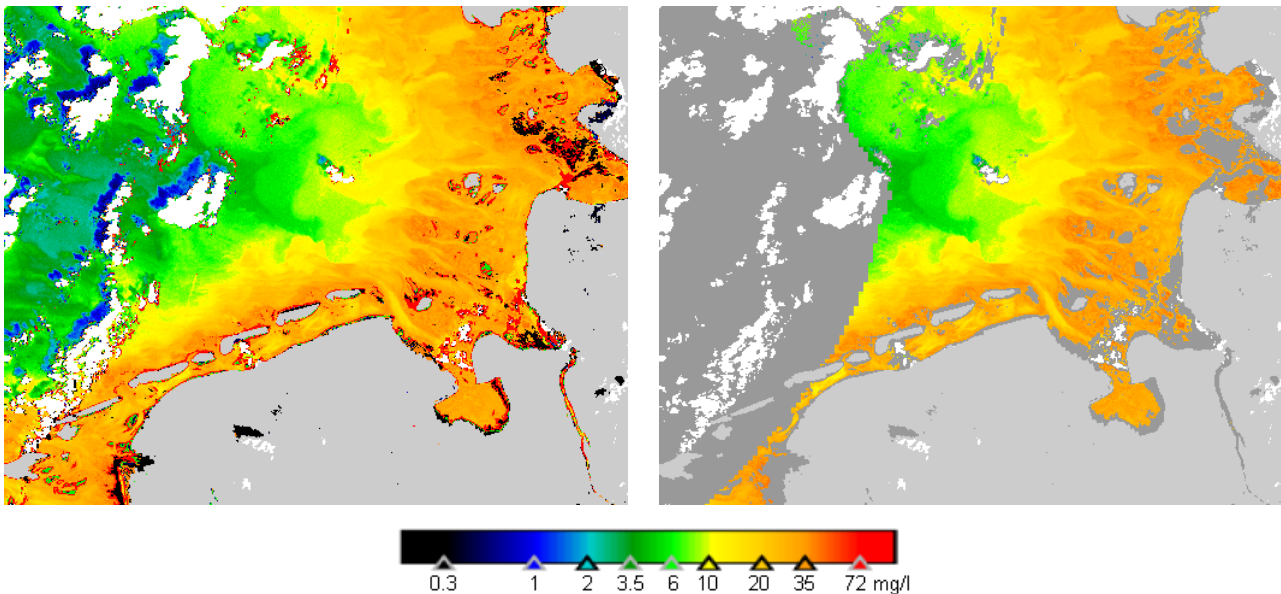


Figure 5: MERIS derived full-resolution TSM concentration image for 19 Feb 2005, during ebb current (3 hours after high tide). A south-west wind was blowing at 5.2 m/s for the last 12 hours, with peak velocity of about 10 m/s the day before. White areas are clouds, the blue parts next to them are their shadows.

In summer, the patterns always show a straight transition of backbarrier water to water of the German Bight, as long as the wind speed is low or moderate. Figure 4 shows the typical “wave-like” patterns evolving during ebb current. During winter, the sharp gradient breaks up and the suspended matter patterns reach deep into the German Bight (examples are given in Figures 5 and 6). Although the wind speed is normally higher in wintertime, these patterns of high suspended matter concentration reaching deeply into the German Bight may not be explained solely by the wind impact. The satellite observations support the hypothesis of a strong dependence of settling velocity on kinematic viscosity, the latter depending on temperature (27,28). As settling velocities are smaller in winter the suspended matter remains in the water column for a longer time, which results in a larger extension of areas with high concentrations. The largest measured value was 300 mg/l

in the Spiekeroog inlet on 20 Jan 2004 (filtration data), during ebb tide, with wind speeds of 5 to 15 m/s the days before.

While the above described patterns are already known from observations and numerical simulations, the pattern shown in Figure 6 seems new. This pattern is characterised by several strips of high concentration originating from the tidal channels and penetrating deep into the German Bight. It seems that these strips with high *TSM* concentration are not directly connected with tidal fronts, which is justified by the lack of correlation of these patterns and topography. A more plausible explanation is that these high-concentration zones are transport patterns from the tidal flats into the North Sea, which are subject to east-west oscillations, the latter modulating the spatial properties of *TSM*.

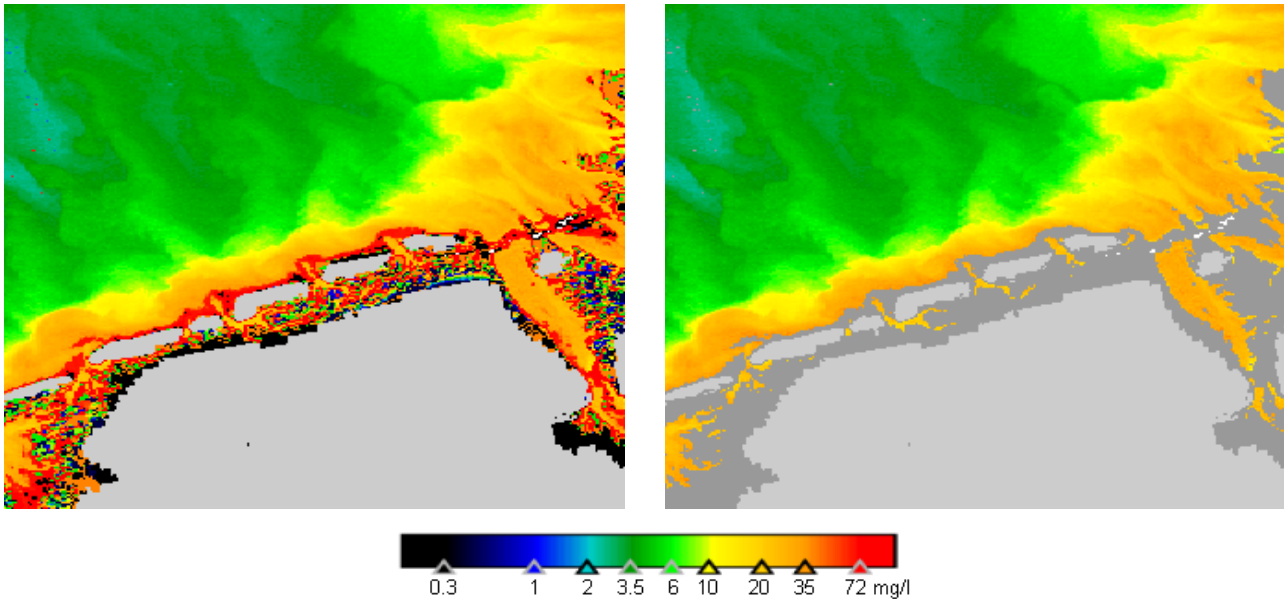


Figure 6: MERIS derived full-resolution *TSM* concentration image for 29 Mar 2004, showing low water. Wind was blowing at 6.3 m/s and from a direction of 227° for at least the last 12 hours. Most areas in the back barrier have fallen dry (dark grey pixels are invalid). The concentrations in the German Bight are high, which is typical for a winter situation. A special feature of this scene is the absence of clouds and the very well developed *TSM* structures, penetrating deeply into the German Bight.

NUMERICAL SIMULATIONS

Model area, discretisation and forcing

The present work uses results of numerical simulations with the General Estuarine Transport Model (GETM), which is a 3-D primitive equation numerical model (29), shortly presented in the Appendix (Figure 7). In this model the equations for the three velocity components, u , v , and w and sea-surface height ζ , as well as equations for the turbulent kinetic energy (*TKE*) k and the eddy dissipation rate (*EDR*) due to viscosity ε are solved. The numerical model is coupled with a sediment transport model, in which mud particles of a grain size of $d = 63 \mu\text{m}$ are considered. The model uses a standard diffusion-advection equation for the concentration of suspended sediment.

The first application of this model to the area of our study is described by (30) and we refer to this paper for more details. The model uses terrain-following equidistant vertical coordinates (σ -coordinates). The vertical column extending from the bottom $-H(x,y)$ to the surface $\zeta(x,y,t)$ is divided into ten non-intersecting layers. With a horizontal resolution of 200 m the area in Figure 1 is resolved with 324×88 grid-points in the zonal and meridional direction, respectively.

The forcing at the open boundaries is taken from the simulations with the operational model of the German Bight provided by the Bundesamt für Seeschifffahrt und Hydrographie, Hamburg, Germany

(BSH) (30). The sea-level data (one value every 15 minutes) have been interpolated in time and space onto the grid points along the boundaries of our regional model. Lateral boundary conditions for concentration are taken to be zero for inflowing water. This agrees with satellite and direct observations demonstrating that concentrations along the northern model boundary are small (at least 5 times smaller than in the tidal basins). Outflowing water results in a suspended matter flux of $u_n c$ out of the model area, where u_n is the velocity normal to the boundary.

Here we will discuss only the results of simulations for the period 16 to 18 October 2000, which are representative for the general conditions during spring tide (see (30) for more details about the results of simulations).

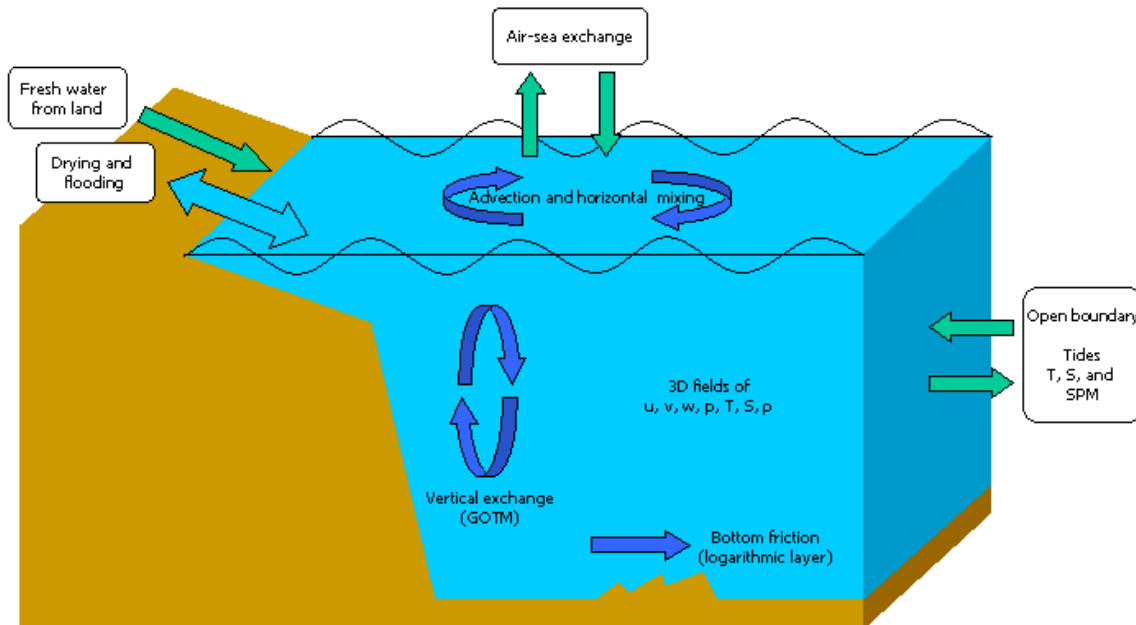


Figure 7: Schematic presentation of the model.

Circulation

Most of the present study is based on the same simulations as reported in the study of (30) and (31) where an extensive validation has been carried out using continuous measurements (ten-minute records) of sea-level and currents (ADCP transects along and across the tidal channels).

The water exchange during one tidal period between open-ocean and backbarrier basin of Spiekerroog amounts to $\approx 100 \cdot 10^6 \text{ m}^3$ and $\approx 140 \cdot 10^6 \text{ m}^3$ during neap and spring tide respectively (7). It is noteworthy that the simulated wet area (Figure 8) varies with time demonstrating that the model resolves one of the most characteristic features of the Wadden Sea, which is the process of flooding and drying.

The circulation (Figure 8) is dominated by a westward transport during ebb and eastward transport during flood. The simulated magnitudes compare well with the observations of (1). It has been demonstrated by (30) and (32) that, while the transport through the inlets is mainly controlled by the up-and-down tidal oscillations, the along-shore circulation, as well as the circulation in the intertidal areas, are controlled by the spatial properties (back-and-forth propagation) of the tidal signal. The maximum ebb velocity is observed in the tidal channels shortly before the rate of sea-level fall reaches its maximum. However, the maximum flood velocity is delayed in the tidal channels by approx. 2 hours with respect to the maximum rate of sea-level rise, which is due to the hypsometric control of basins with time-variable horizontal area. This asymmetry is also known as "shorter-falling" asymmetry (in the terminology of (33)). As asymmetries in the tidal response are indicative for the transports during flood and ebb (34), shorter-falling and shorter-rising asymmetries are used sometimes as synonymous for an ebb and flood dominated regime, correspondingly.

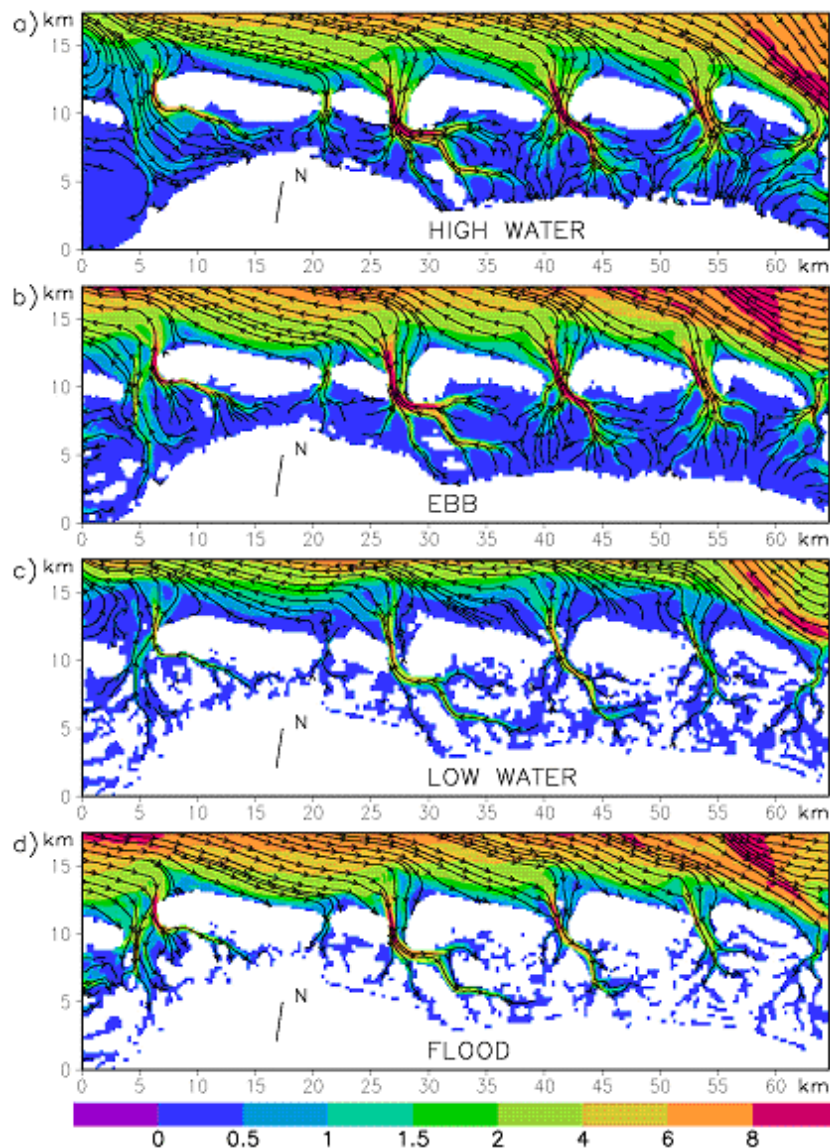


Figure 8: Vertically integrated velocity simulated during high water (a), ebb (b), low water (c), and flood (d) phases of spring tidal cycle. These four stages are identified by the position of tide at the northern boundary, which explains why the largest drying of tidal flats is delayed with respect to the low water.

Sediment dynamics

The surface concentration of fine suspended matter (Figure 9) reveals two distinct areas with high values: in the tidal inlets and north of the back barrier islands. In both areas the depth is relatively large (see Figure 1), which could partially explain the large mass of suspended matter fractions there.

During flood the "sediment clouds" north of the islands are displaced slightly southwards. However, instead of "entering" the back barrier basin (being its origin) through the tidal inlet, part of the suspended matter moves eastwards, the "sediment clouds" reaching their easternmost displacement during high water (Figures 8a and 9a), which is in the middle of the northern coast of the islands.

These results indicate that the strongest signal in the sediment dynamics is associated with the oscillation of sediment pools in east-west direction. In this signal the dominating period is the tidal one, not the semi-tidal one, the latter being associated with vigorous erosion/deposition (7).

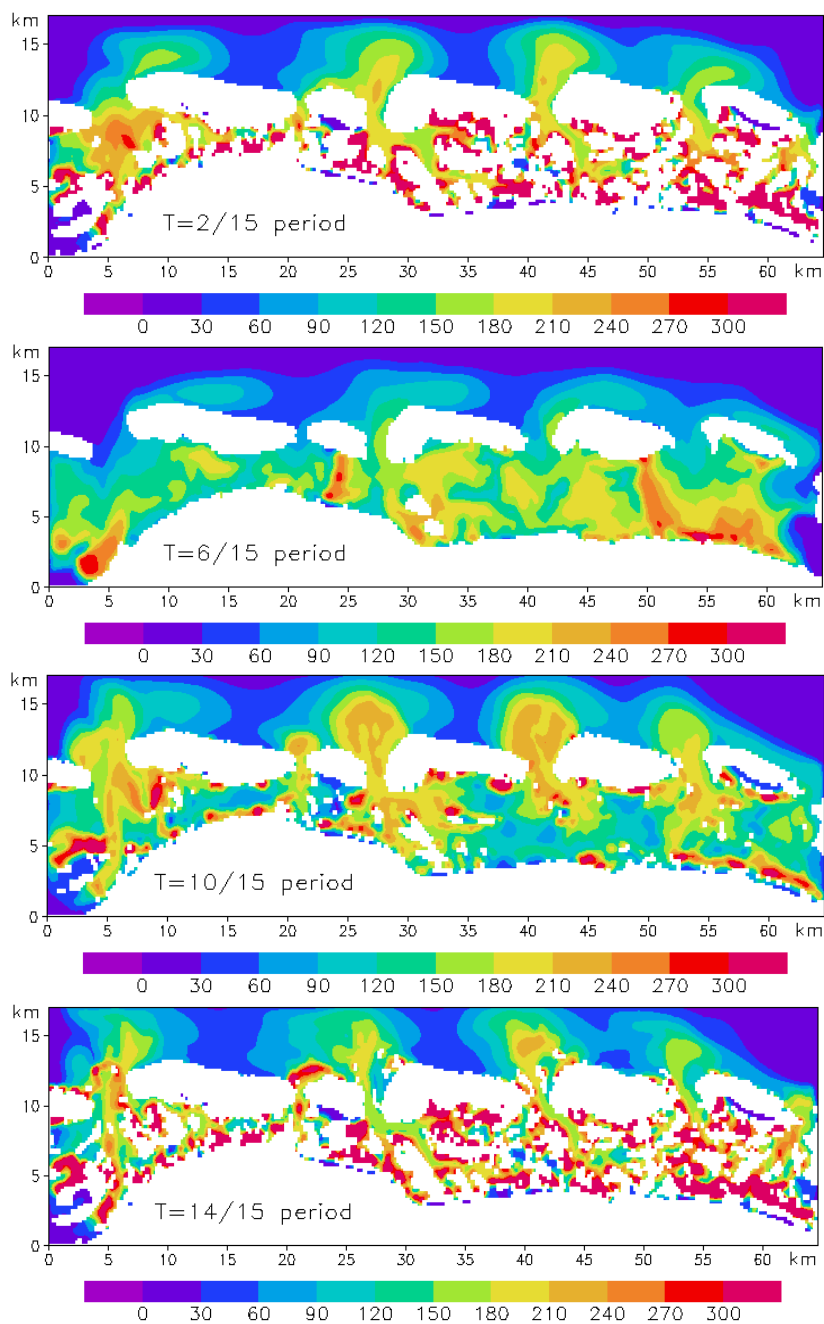


Figure 9: Model results of TSM surface concentrations in arbitrary units. The consecutive plots correspond to the times of flood, high water, ebb, and low water.

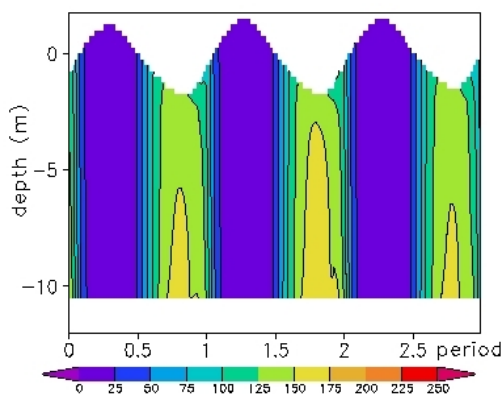


Figure 10: Numerically simulated vertical TSM profiles (in relative units), north of Otzumer Balje.

The fine *TSM* concentrations during high water are only half as large as during flood and ebb (Figure 10). The concentrations during low water reveal absolute maxima north of the barrier islands. These large concentrations are due to the fact that during ebb the waters in the channels (and north of them) are replaced by relatively particle-rich water from the tidal flats.

COMPARISON OF NUMERICAL SIMULATIONS WITH MERIS DATA

In the following, we provide a short demonstration of consistence between the two data types analysed in the present study. We are using a cloud-free MERIS scene (Figure 12) with valid pixels over nearly the whole area. For this period the wind velocity was low for at least the last 12 hours (3.5 m/s) and had an east/north-east direction. The influence of the wind is considered negligible at such low wind velocities. The chosen scene is a high water scene ensuring a water coverage of the whole area. The high water situation together with the above-mentioned low Secchi depths also ensures that MERIS does not see any seafloor shining through the water column, except perhaps at locations very close to the coasts (compare Figure 1).

The corresponding *TSM* distribution calculated by the numerical model is shown in Figure 11. For this first test, the *TSM* concentrations were not calibrated yet, because the main issue was to compare the *TSM* distribution between the simulation and the MERIS data.

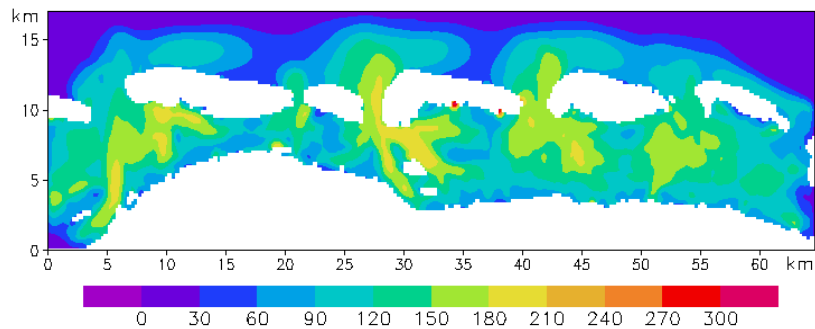


Figure 11: *TSM* distribution in arbitrary units at the sea surface at high water, simulated by the sediment transport model.

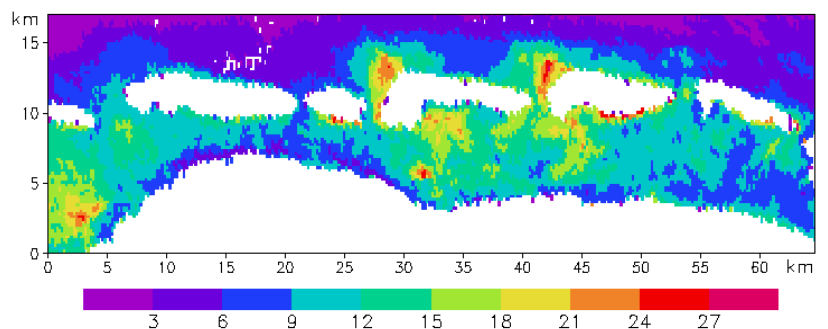


Figure 12: MERIS image of the 3 Jun 2004, *TSM* in mg/l. Only values of less than 30 mg/l are considered due to the uncertainties of the present algorithm at higher concentrations.

The investigation shown here considers the main cross-shore distribution pattern of *TSM*. In Figure 13 we compare the satellite and model data of the mean concentrations along transects parallel to the coast. The distances from the coast are equivalent to the distances in Figures 11 and 12.

Although slightly shifted, all changes of the slope of curves seen in observations are replicated in the numerical model. The detailed horizontal patterns match well in the two datasets (Figure 13).

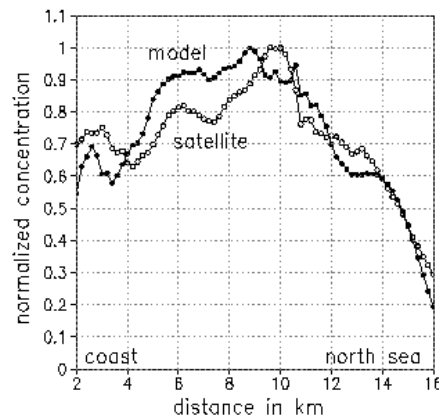


Figure 13: Comparison of MERIS image and model, mean TSM values of east-west transects parallel to the coast (normalised with respect to the maximum).

CONCLUSIONS

The simulations with a 3-D hydrodynamic model coupled with a sediment transport model help to further understand the dominant patterns. It has been shown that "sediment clouds" north of the barrier islands represent one of the most important elements of the sediment dynamics in the region. Their oscillation in the east-west direction is dominated by tidal periodicity (not a semi-tidal one, the latter being associated with vigorous erosion/deposition). By circulating around the islands fine TSM undergoes complicated transformations resulting from erosion and deposition in quite different areas during different parts of the tidal cycle.

This first comparison is a preliminary one. Further and more detailed investigations are necessary. Nevertheless, with this result we show that the numerical model has been validated with the observed concentrations of MERIS in principle. The good qualitative consistence of observed to model data is encouraging further investigation.

The satellite images indicate a strong dependence of the suspended matter on seasonal factors due to meteorological conditions. To investigate this behaviour in a more detailed way, the model has to be run in a much larger area, as the winter satellite data prove. Secondly, for quantitative comparisons of cases the model setups have to be prepared consistent with the realistic (individual) situations. This includes e.g. wind impact, which may be an important factor for the TSM concentrations particularly for special environmental situations such as storms. These aspects along with others will be addressed in a future study.

APPENDIX: THE NUMERICAL MODEL

Circulation model

The present work uses results of numerical simulations with the General Estuarine Transport Model (GETM) coupled with a sediment transport module. GETM is a 3-D primitive equation numerical model (29), in which the momentum and continuity equations in Cartesian co-ordinates read:

$$\frac{\partial u}{\partial t} + \gamma \left(\frac{\partial(u^2)}{\partial x} + \frac{\partial(uv)}{\partial y} - fv + \frac{\partial(uw)}{\partial z} \right) = -g \frac{\partial \zeta}{\partial x} + \frac{\partial}{\partial z} \left(A_V \frac{\partial u}{\partial z} \right) + A_H \nabla^2 u \tag{1}$$

$$\frac{\partial v}{\partial t} + \gamma \left(\frac{\partial(uv)}{\partial x} + \frac{\partial(v^2)}{\partial y} + fu + \frac{\partial(vw)}{\partial z} \right) = -g \frac{\partial \zeta}{\partial y} + \frac{\partial}{\partial z} \left(A_V \frac{\partial v}{\partial z} \right) + A_H \nabla^2 v \tag{2}$$

$$\frac{\partial u}{\partial x} + \frac{\partial v}{\partial y} + \frac{\partial w}{\partial z} = 0 \tag{3}$$

where u , v , and w are the velocity components with respect to the x (east), y (north), and z (upward) direction, f is the Coriolis parameter, g the acceleration due to gravity, ζ the sea-surface height, $A_V(k, \varepsilon, \gamma)$ a generalised form of the vertical eddy viscosity coefficient, k the turbulent kinetic energy (*TKE*) per unit mass, and ε the eddy dissipation rate (*EDR*) due to viscosity. The lateral eddy viscosity $A_H(x, y)$ has been introduced to suppress non-physical noise along the open boundaries in a three grid-point wide sponge layer, where it changes exponentially from its boundary value of $10^3 \text{ m}^2\text{s}^{-1}$ to $1/e$ of this value. In the interior of the model domain the dissipation is dominated by vertical friction.

The success of near coastal models in tidal basins depends largely on the capabilities of modelling the process of drying and flooding adequately. In GETM, this process is incorporated in the hydrodynamical equations through a parameter γ that equals unity in regions where a critical water depth D_{crit} is exceeded and which approaches zero when the thickness of the water column $D = H + \zeta$ tends to a minimum value D_{min} :

$$\gamma = \min\left(1, \frac{D - D_{min}}{D_{crit} - D_{min}}\right) \quad (4)$$

where H is the local depth (constant in time), taken as the bottom depth below mean sea-level in the model area. The minimum allowable thickness D_{min} of the water column is 2 cm and the critical thickness D_{crit} is 10 cm (29,32). For a water depth greater than 10 cm ($D \geq D_{crit}$ and $\gamma = 1$), the full physics is included. In the range between critical and minimal thickness (between 10 and 2 cm) the model physics are gradually switched towards friction domination, i. e. by reducing the effects of horizontal advection and Coriolis acceleration in Eqs. (1) and (2) and varying the vertical eddy viscosity coefficient A_V according to

$$A_V = \nu_t + (1 - \gamma)\nu_b \quad (5)$$

where $\nu_b = 10^{-2} \text{ m}^2\text{s}^{-1}$ is a constant background viscosity. The eddy viscosity ν_t is obtained from the relation

$$\nu_t = c_\mu^4 \frac{k^2}{\varepsilon} \quad (6)$$

where $c_\mu = 0.56$ (see e. g. (35)).

In GETM, the momentum equations, Eqs. (1) and (2), and the continuity equation, Eq. (3), are supplemented by a pair of equations describing the time evolution of the *TKE* and *EDR*:

$$\frac{\partial k}{\partial t} - \frac{\partial}{\partial z} \left(\frac{\nu_t}{\sigma_k} \frac{\partial k}{\partial z} \right) = P - \varepsilon \quad (7)$$

$$\frac{\partial \varepsilon}{\partial t} - \frac{\partial}{\partial z} \left(\frac{\nu_t}{\sigma_\varepsilon} \frac{\partial \varepsilon}{\partial z} \right) = \frac{\varepsilon}{k} (c_1 P - c_2 \varepsilon) \quad (8)$$

where σ_k and σ_ε are the turbulent Schmidt numbers, $c_1 = 1.44$, and $c_2 = 1.92$ (see (29,32,35)).

The vertical shear production P is a function of the shear frequency S :

$$P = \nu_t S^2 \quad (9)$$

with

$$S^2 = \left(\frac{\partial u}{\partial z} \right)^2 + \left(\frac{\partial v}{\partial z} \right)^2 \quad (10)$$

There is clear observational evidence that the velocity profiles close to the bottom in the East Frisian Wadden Sea may be adequately described by a logarithmic boundary layer (36,37):

$$\frac{u(z')}{u_*^b} = \frac{1}{\kappa} \ln\left(\frac{z'+z_o}{z_o}\right) \quad (11)$$

where $u_*^b = \sqrt{\frac{\tau_b}{\rho_w}}$ is the friction velocity at the sea floor, $\tau_b = \rho_w \nu_t \frac{\partial u}{\partial z}$ is the bed shear-stress, z' is the distance from the bed, z_o is the bottom roughness length, κ is the von Karman constant, and ρ_w is the water density.

Furthermore, close to the bed, *TKE* and *EDR* are governed by the law of the wall with

$$k = \frac{(u_*^b)^2}{c_\mu^{1/2}}, \quad \varepsilon = \frac{(u_*^b)^3}{\kappa(z'+z_o)} \quad (12)$$

Boundary conditions for Eqs. (7) and (8) are described in detail by (29) and (32) along with the parameterisations used. The parameter z_o , which gives a general representation of the bottom roughness, is taken constant over the whole area (32).

The impact of wind waves on the sedimentary system in the same area is addressed earlier by (38), where it has been demonstrated that breaking wind waves affect suspended matter concentrations considerably, in particular on the shallows (usually in the backbarrier basins). Because in the present study we focus on suspended matter patterns north of the barrier islands, and because winds are relatively weak for most cases addressed here, we do not account for the effect of wind waves, assuming that model forcing is dominated by moderate winds (magnitude of 5 m/s) in the region of interest.

The sub-grid scale parameterisations are of utmost importance for the sediment transport, and the analysis of simulations by (32) demonstrates that the general characteristics of turbulence in the bottom boundary layer are consistent with the requirements formulated by (39) for correct prediction of suspended matter transport rates. Two of them are the logarithmic velocity profile and the parabolic-like distribution of A_v .

Sediment transport model

In the sediment transport model, mud particles of a grain size of $d = 63 \mu\text{m}$ are considered. The model uses a standard diffusion-advection equation for the concentration c :

$$\frac{\partial c}{\partial t} + u \frac{\partial c}{\partial x} + v \frac{\partial c}{\partial y} + w \frac{\partial c}{\partial z} = \frac{\partial c}{\partial z} \left(A_v \frac{\partial c}{\partial z} \right) + \frac{\partial}{\partial z} (w_s c) \quad (13)$$

In the above equation, w_s is the settling velocity of the sediment in suspension. For the cohesive sediments, which include mud particles and parts of the silt fraction, the settling velocity is concentration- dependent.

In the following, we present first the parameterisations associated with the cohesive sediments, which we refer to as fine suspended particulate matter (SPM, $d < 63 \mu\text{m}$). Higher concentrations result in a formation of larger aggregates, which in turn have a higher settling velocity. Experiments reveal a strong increase of the settling velocity with the suspended matter concentration (40), which is expressed by the relation

$$w_s = k_s c_{nd}^{m_s} \quad (14)$$

where $c_{nd} = c/c_{un}$ is a non-dimensional concentration of the grain size in question, $c_{un} = 1 \text{ kg/m}^3$, and k_s and m_s are empirical constants. These are chosen to be $k_s = 0.017 \text{ ms}^{-1}$ and $m_s = 1.33$ in agreement with the measurements summarised in (40).

The sediment flux at the sea bed

$$\left(A_V \frac{\partial c}{\partial z} + w_s c \right)_{z=-H} = E - D \quad (15)$$

which is the bottom boundary condition of Eq. (13), is based on well-known parameterisations of deposition and erosion rates D and E . The deposition rate given by Einstein and Krone (41) is

$$D = w_s c_b \left(1 - \frac{\tau_b}{\tau_d} \right) \quad (16)$$

where c_b is the fine SPM concentration near the bottom, τ_b is the bed shear stress and τ_d is the critical shear stress for deposition.

The erosion rate is computed using the formula of (42):

$$E = \alpha M_e \left(\frac{\tau_b}{\tau_e} - 1 \right) \quad (17)$$

where M_e is an empirical constant giving the erosion rate at twice the critical shear stress for erosion. The parameter α specifies the fraction of the grain size in the bottom sediment and is 0.5. The value used for M_e is $3.7 \cdot 10^{-6} \text{ kgm}^{-2}\text{s}^{-1}$. This is somewhat smaller than the values suggested by other authors, e.g. (43,44,45), ranging between $6 \cdot 10^{-6}$ and $4 \cdot 10^{-3} \text{ kgm}^{-2}\text{s}^{-1}$, but showed good results in initial model runs.

The critical shear stress for erosion of fine SPM is set constant to 0.2 Nm^{-1} . The critical shear stress for deposition is chosen to be equal to that for erosion. That means that either deposition or erosion occurs and no region of transition exists where none of the two processes are active.

The sediment source at the bottom is taken (as a first order approximation) to be inexhaustible everywhere. If the water depth equals D_{\min} the location is considered dry and the sediment equations are not solved anymore until the water depth increases again.

ACKNOWLEDGEMENTS

We would like to thank the European Space Agency ESA for providing the MERIS data within Category-1 Project No. 1359 *Budget and States of the Wadden Sea Tidal Flat Water Column*.

We are indebted to H. Burchard and K. Bolding for making GETM available to us. The stimulating discussions with B. Flemming were highly appreciated.

REFERENCES

- 1 Santamarina Cuneo P & B Flemming, 2000. Quantifying the concentration and flux of suspended particulate matter through a tidal inlet of the East Frisian Wadden Sea by acoustic Doppler current profiling. In: Muddy Coast Dynamics and Resource Management, edited by B W Flemming, M T Delafontaine & G Liebezeit (Elsevier Science, Amsterdam, The Netherlands) 39-52
- 2 Barth H, R Reuter & M Schröder, 2001. [Measurement and simulation of substance specific contributions of phytoplankton, gelbstoff and mineral particles to the underwater light field in coastal waters](#). EARSeL eProceedings, 1: 165-174
- 3 IOCCG, 2000. [Remote sensing of ocean colour in coastal, and other optically-complex waters](#). Edited by S Sathyendranath. Reports of the International Ocean-Colour Coordinating Group (IOCCG), No. 3 (Dartmouth, Canada) 140 pp.

- 4 IOCCG, 2004. [Guide to the creation and use of ocean-colour, Level-3, binned data products](#). Edited by D Antoine. Reports of the International Ocean-Colour Coordinating Group (IOCCG), No. 4 (Dartmouth, Canada) 88 pp.
- 5 [Data of coastal time-series stations](#), 1999. (GKSS Research Centre, Geesthacht, Germany)
- 6 [Time-Series Station Wattenmeer](#), 2002. (Carl von Ossietzky University of Oldenburg, Germany)
- 7 Stanev E V, G Brink-Spalink & J-O Wolff, 2006. Sediment dynamics in tidally dominated environments controlled by transport and turbulence. A case study for the East Frisian Wadden Sea. Manuscript submitted to [Journal of Geophysical Research](#)
- 8 Gordon H R, 1997. Atmospheric correction of ocean color imagery in the Earth Observing System era. [Journal of Geophysical Research](#), 102(D14): 17,081-17,106
- 9 Doerffer R, K Sorensen & J Aiken (1999). MERIS potential for coastal zone applications. [International Journal of Remote Sensing](#), 20(9): 1809-1818
- 10 Doxaran D, S J Lavender & J-M Froidefond, 2004. [Mapping tidal and seasonal movements of the maximum turbidity zone in estuarine waters from remotely sensed \(SPOT, LANDSAT\) data](#). A semi-empirical approach. [EARSeL eProceedings](#), 3(1): 54-68
- 11 Lehner S, I Anders & G Gayer, 2004. [High resolution maps of suspended particulate matter concentration in the German Bight](#). [EARSeL eProceedings](#), 3(1): 118-126
- 12 IOCCG News, [June 2004](#); CONAE Catalogue of Products, [Satellite SAC-C, Camera: MMRS](#)
- 13 Navalgund R R and A S Kiran Kumar. [Ocean Colour Monotor \(OCM\) on Indian Remote Sensing Satellite IRS-P4](#). IOCCG
- 14 [MERIS Product Handbook, Chapter 3.1](#). European Space Agency ESA, 2004
- 15 [The Beam Project](#), 2002. (Brockmann Consult, Geesthacht, Germany)
- 16 Goryl P (2005) [MERIS / AATSR Processor and Operation History](#). [MERIS – \(A\)ATSR Workshop](#) 26-30 Sept 2005 (ESA, ESRIN)
- 17 Bourg L & G Obolensky, 2006. [Evolution of the MERIS instrument processing facility](#) European Space Agency, Technical Note 2.0, April 2006, 12 pp.
- 18 Doerffer R & H Schiller, 1997. [Algorithm Theoretical Basis Document \(ATBD 2.12\)](#): Pigment index, sediment and gelbstoff retrieval from directional water leaving radiance reflectances using inverse modelling technique. European Space Agency, Doc. No. PO-TN-MEL-GS-0005
- 19 Bourg L, S Delwart & J-P Huot (2002) [Calibration of MERIS on ENVISAT: Status at end of 2002](#). In: [Proceedings of Envisat Validation Workshop](#), 9-13 Dec 2002 (ESA, ESRIN) 15 pp.
- 20 Doerffer R & H Schiller (2005) [MERIS for Case-2 Waters](#). [MERIS – \(A\)ATSR Workshop](#) 26-30 Sept 2005 (ESA, ESRIN)
- 21 Goryl P (2005) [MERIS / AATSR Processor and Operation History](#). [MERIS – \(A\)ATSR Workshop](#) 26-30 Sept 2005 (ESA, ESRIN)
- 22 Pasterkamp R, S W M Peters & J H Van der Woerd (2003). [MERIS validation of geophysical ocean colour products: preliminary results for the Netherlands](#). In: [Proceedings of Envisat Validation Workshop](#), 9-13 December 2002, Frascati, Italy (ESA SP-531, March 2003), edited by H Lacoste (ESA Publications Division, Noordwijk, The Netherlands) 8 pp.
- 23 Ruddick K, V de Cauwer, Y Park, G Becu, J-P de Blauwe, E De Vreker, P-Y Deschamps, M Knockaert, B Nechad, A Pollentier, P Roose, D Saudemont & D Van Tuyckom (2003) [Preliminary validation of MERIS water products for Belgian coastal waters](#). In: [Proceedings of](#)

- [Envisat Validation Workshop](#) 9-13 December 2002, Frascati, Italy (ESA SP-531, March 2003), edited by H Lacoste (ESA Publications Division, Noordwijk, The Netherlands) 15 opp.
- 24 [MERIS Product Handbook](#), [Chapter 2.7.1.3](#): Level 2 Accuracies. European Space Agency ESA, 2004
- 25 Lunau M, A Lemke, O Dellwig & M Simon, 2006. Physical and biogeochemical controls of microaggregate dynamics in a tidally affected coastal ecosystem. [Limnology and Oceanography](#), in press
- 26 Chang T, A Bartholomae & B Flemming, 2006. Seasonal dynamics of fine-grained sediments in a back-barrier tidal basin of the German Wadden Sea (southern North Sea). [Journal of Coastal Research](#), in press
- 27 Krögel F & B W Flemming, 1998. Evidence for temperature adjusted sediment distribution in the back-barrier tidal flats of the East Frisian Wadden Sea (southern North Sea). In: [Tidalites: processes and products](#), edited by C R Alexander, R A Davis & V J Henry. SPEM Pub 61: 31-41
- 28 Flemming B W, 2004. [Factors affecting the shape of particle frequency distribution and associated textural parameters](#). In: [From particle size to sediment dynamics](#), edited by B W Flemming. International Workshop at the Hanse Institute of Advanced Studies, 15-18 April 2004 (Delmenhorst, Germany) 53-58
- 29 Burchard H & K Bolding, 2002. [GETM - a general estuarine transport model](#). Scientific Documentation, No EUR 20253 EN (European Commission) 157 pp.
- 30 Dick S K, K Eckard, S H Müller-Navarra, H Klein & H Komo, 2001. The operational circulation model of BSH (BSHcmod) - Model description and validation. [Berichte des Bundesamtes für Seeschifffahrt und Hydrographie \(BSH\)](#): 29, 49 pp.
- 31 Stanev E V, G Flöser & J-O Wolff, 2003. Dynamical control on water exchanges between tidal basins and the open ocean. A Case Study for the East Frisian Wadden Sea. [Ocean Dynamics](#) 53: 146-165
- 32 Stanev E V, J-O Wolff, H Burchard, K Bolding & G Flöser, 2003. On the Circulation in the East Frisian Wadden Sea: Numerical modeling and data analysis. [Ocean Dynamics](#), 53: 27-51
- 33 Friedrichs C T & O S Madsen, 1992. Nonlinear diffusion of the tidal signal in frictionally dominated embayments. [Journal of Geophysical Research](#), 97 C4: 5637-5650
- 34 Groen P, 1967. On the residual transport of suspended matter by an alliterating tidal current. [Netherlands Journal of Sea Research](#), 3: 564-574
- 35 Rodi W, 1980. Turbulence models and their application in hydraulics. Rep International Association for Hydraulic Research (Delft, The Netherlands) 104 pp.
- 36 Davis R A Jr. & B Flemming, 1991. Time-series study of mesoscale tidal bedforms, Martens Plate, Wadden Sea, Germany. In: [Clastic Tidal Sedimentology](#), edited by D G Smith, G E Reinson, B A Zaitlin & R A Rahmani (Canadian Society of Petroleum Geologists) Memoir 16: 275-282
- 37 Antia E E, 1993. Sedimentology, morphodynamics and facies association of a mesotidal barrier and island shoreface (Spiekeroog, Southern North Sea). [Berichte aus dem Fachbereich Geowissenschaften der Universität Bremen](#) 32: 370 pp
- 38 Stanev E V, G Brink-Spalink & J-O Wolff, 2004. On the sensitivity of sediment system in the East Frisian Wadden Sea to climate change, In: [Klimaänderung und Küstenschutz](#), edited by G Goennert, H Grassl, D Kellat, D Kuntz, B Probst, H von Storch & J Sündermann, 62-72

- 39 Dyer K R & R L Soulsby, 1988. Sand transport on the continental shelf. Annual Review of Fluid Mechanics, 20, 295-324
- 40 van Leussen W, 1988. Aggregation of particles, settling velocity of mud flocks. In: Physical Processes in Estuaries, edited by J Dronkers & W van Leussen (Springer, Heidelberg) 347-404
- 41 Einstein H A & R B Krone, 1962. Experiments to determine modes of cohesive sediment transport in salt water. Journal of Geophysical Research, 67: 1451-1461
- 42 Partheniades E, 1965. Erosion and deposition of cohesive soils. Journal of the Hydraulic Division, ASCE, 91(HY1)
- 43 Mehta A J, 1988. Laboratory studies on cohesive sediment deposition and erosion. In: Physical Processes in Estuaries, edited by J Dronkers & W van Leussen (Springer, Heidelberg) 327-345
- 44 Puls W & J Sündermann, 1990. Simulation of suspended sediment dispersion in the North Sea. In: Coastal and Estuarine Studies, Vol. 38: Residual Currents and Long-term Transport, edited by RT Cheng (Springer, New York) 356-372
- 45 Clarke S & A J Elliot, 1998. Modelling suspended sediment concentrations in the Firth of Forth, Estuarine, Coastal and Shelf Science, 47: 235-250